

Ising model on a 2D *additive* Small-World Network

R. A. Dumer* and M. Godoy†

Instituto de Física - Universidade Federal de Mato Grosso, 78060-900, Cuiabá, Mato Grosso, Brazil.

In this article, we have employed Monte Carlo simulations to study the Ising model on a two-dimensional *additive* small-world network (A-SWN). The system model consists of a $L \times L$ square lattice where each site of the lattice is occupied for a spin variable that interacts with the nearest neighbor and has a certain probability p of being additionally connected at random to one of its farther neighbors. The system is in contact with a heat bath at a given temperature T and it is simulated by one-spin flip according to the Metropolis prescription. We have calculated the thermodynamic quantities of the system, such as, the magnetization per spin m_L , magnetic susceptibility χ_L , and the reduced fourth-order Binder cumulant U_L as a function of T for several values of lattice size L and additive probability p . We also have constructed the phase diagram for the equilibrium states of the model in the plane T versus p showing the existence of a continuous transition line between the ferromagnetic F and paramagnetic P phases. Using the finite-size scaling (FSS) theory, we have obtained the critical exponents for the system, where varying the parameter p , we have observed a change in the critical behavior from the regular square lattice Ising model to A-SWN.

I. INTRODUCTION

At the beginning of the century, the Small-World effect observed by Milgram [1] came to prominence after Watts and Strogatz [2] quantify their structural properties through graph theory. The Watts-Strogatz model [2] (WS-model) is based on the idea that the vertices of a graph are the network sites, and the edges are connections between two sites of this network. As well, by introducing a disorder parameter p , as the probability of rewriting randomly each one of the connections in a regular lattice, we obtain the small-world network (SWN) in specific regions of the interval $0 < p \leq 1$. These regions of p in which we have the SWN regime, it is identified when the network has the local clustering of a regular lattice, but at the same time have an average distance between any two sites of the network characteristic of a random lattice [2].

The structural properties of the WS-model were investigated [2–7] and applied in the study of the disease transmission with the probability reaching the epidemic behavior [2, 4, 8], once in the Milgram experiment [1] is suggested that on average, exist six intermediaries separating two people in the world, inducing that one high infectious disease could spread across the whole planet in about six incubation periods for the disease [8].

In addition to the WS-model, some variants of this model were also developed to describe the properties of an SWN. In one of these variants [4], there is a regular square lattice where each site has n edges, i.e., degree n , and with a certain probability p is possible to add long-range interactions to each site in the network, being each site able to receive n long-range interactions. Therefore, we can obtain a small typical separation, while the clustering property of the regular lattice is always preserved.

A simplified version of this variant can be made if we decrease the number of long-range interactions that each site can receive. These variants are called *additive* SWN (A-SWN), while we have the in the WS-model we have defined the *rewiring* SWN (R-SWN) [2].

Since the first SWN model was proposed, these networks have been implemented in a variety of physical models [9–12], including the Ising model, which was studied by Monte Carlo simulations with the A-SWN in 1D [13, 14] and with the R-SWN in 1D, 2D e 3D [15, 16]. We also have exact and approximate analytical results for the A-SWN and R-SWN in 1D [5, 17, 18]. These results in 1D show that an ordered to the disordered phase transition is obtained for $T \neq 0$ with $0 < p \leq 1$, and for 1D, 2D e 3D is observed a change in the critical behavior of the system by the addition of long-range interactions.

In this work, we have investigated the Ising model in a two-dimensional A-SWN, where each site of the network is occupied by a spin variable $\sigma = 1/2$ that can assume values ± 1 . We limit by one the number of long-range interactions that each site can receive with probability p and dividing our network in two sublattices, each new interaction created should connect these sublattices. A similar model was proposed by Zhang and Novotny [19] in his SW-model, where the long-range interactions are completely random and always present on all sites of the network, i.e., p is always 1. They have found a mean-field critical behavior in his model, so here we will verify if the limitation on the randomness of the long-range interactions changes the predicted mean-field critical behavior for $p = 1$, and what is the critical behavior of the system in other points of the A-SWN regime, i.e., other regions of p where the A-SWN behavior is also observed.

This article is organized as follows: In Section II, we describe the network used and the Hamiltonian model of the system. In Section III we present the Monte Carlo simulation method used, some details concerning the simulation procedures, and the thermodynamic quantities of the system necessary for the application of FSS analysis. The behavior of the phase transitions, phase diagrams,

* rafaeldumer@fisica.ufmt.br

† mgodoy@fisica.ufmt.br

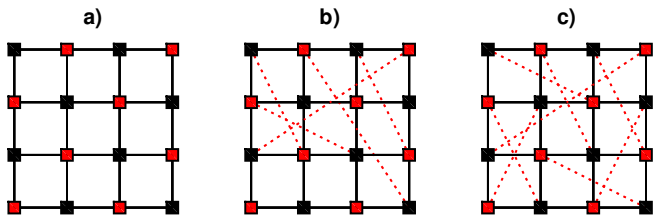


Figure 1. Schematic representation of the system and the A-SWN. The black square dots indicate the sites on one of the sublattices, the red square dots are the sites on the other sublattice, the solid black lines are the nearest-neighbor interactions J between pairs of spins, and the red-dashed lines are long-range interaction J_{ik} added to the network with a certain probability p . In a) we have $p = 0$, i.e., the probability of adding a long-range interaction J_{ik} to any site on the lattice is zero, therefore, we have a regular square lattice. b) $p = 0.5$, we are in the A-SWN regime because in addition to the conservation of $C(p)$, and we also have an average the short path length between network sites, through the shortcuts created by the long-range interaction J_{ik} added between the sublattices. c) $p = 1$, all sites on the network have a long-range interaction J_{ik} connecting the two sublattices, and consequently, it is the network with the shortest typical separation between the sites on the network.

and critical exponents by FSS analysis are described in Section IV, and finally, in Section V we present our conclusions.

II. MODEL

In this work, the studied model is the Ising model with $N = L^2$ spins $\sigma_i = \pm 1$ on a regular square lattice $L \times L$, with periodic boundary conditions, and a nearest-neighbor ferromagnetic interaction of strength J (see Fig. 1(a)). On the other hand, using the same regular square lattice $N = L \times L$, with a certain probability p , we can add one long-range interaction J_{ik} to each site of the lattice. To add the long-range interaction J_{ik} , we divide the system in two sublattices, where one sublattice plays the role of central spins, while the other sublattice contains the spins in which the central spins can connect, beyond the nearest neighbors. Thus, to choose a long-range interaction J_{ik} for a site i , the sublattice of i will be the sublattice of the central spins, then, we choose randomly a site k from another sublattice. If the site k does not be one of its nearest neighbors already naturally coupled with i , we picked a random number $0 < r < 1$, and if $r \leq p$ (with p predefined), we couple the site k to the neighbors of the site i , and for the site k we couple the site i to its neighbors. The try to add a long-range interaction J_{ik} is made once to each site that do not have a long-range interaction J_{ik} in the network, and as result we have a network with average coordination number $z = 4 + p$.

We can see the evolution of the system for some values of $p \neq 0$ (see Fig. 1(b) and (c)). To reach the A-SWN state as defined in WS-model with the R-SWN, we need

to have two structural properties on the network: 1) a high clustering coefficient $C(p)$, which is characteristic of regular lattices and is defined as the ratio between the number of connections among neighbors at any site of the network and the possible number of connections among this quantity of neighbors. 2) a small characteristic length path $l(p)$, which is observed in random networks and defined as the shortest distance between two any sites of the network.

Thus, as our regular structure in $p = 0$ keeps unaltered, we have a high $C(p)$ for any value of p , and conform we increase p , the long-range interaction J_{ik} is added to the network, creating shortcuts between the sites that before in the simple regular lattice would be more distant, consequently decreasing the $l(p)$ of the network. The $l(p)$ scales linearly $l(p \rightarrow 0) \sim L/2$, and logarithmically $l(p \rightarrow 1) \sim \ln(L^{1.77})$, being these regimes referred as the “large-world” and “small-world” respectively. The cross-over between these regimes occurs when the average number of shortcuts is about one, or in the other words, we can say in the SWN regime when $p \gtrsim L^{-2}$ [4]. Versed on this, our study is based on $p \geq 0.25$ values, where the A-SWN is found and the decay of l as a function of p undergoes less, i.e., having approximately the same value of l .

The ferromagnetic Ising spin energy is described by the Hamiltonian of the form

$$\mathcal{H} = -J \sum_{\langle i,j \rangle} \sigma_i \sigma_j - \sum_{\langle i,k \rangle} J_{ik} \sigma_i \sigma_k, \quad (1)$$

where J is the nearest-neighbor ferromagnetic interaction, J_{ik} is the long-range interaction on the A-SWN. The first sum is over all the pair of nearest-neighbor spins on the square regular lattice and the second sum is made over all the pairs of spins (i, k) connected through long-range interaction on the A-SWN.

The long-range interaction J_{ik} is distribute randomly and satisfy the following probability distributions:

$$P(J_{ik}) = (1 - p)\delta(J_{ik} - 0) + p\delta(J_{ik} - J), \quad (2)$$

where the term $(1 - p)\delta(J_{ik} - 0)$ indicated that one fraction $(1 - p)$ of pairs of spins (i, k) on the lattice are free of the long-range interactions, while the terms $p\delta(J_{ik} - J)$ indicated that one fraction p of pairs of spins (i, k) are connected through a long-range interaction. Here, we always are considering $J_{ik} = J = 1$.

III. MONTE CARLO SIMULATIONS

We simulate the system specified by the Hamiltonian in Eq. (1) on a $L \times L$ square lattice under periodic boundary conditions applied in all directions. We have chosen the initial state of the system with all spins aligned in the same direction, and a new configuration is generated by the following Markov process: for a given temperature T

and an additive probability p , we choose a random spin σ_i from the square lattice, and then run the one-spin flip dynamic. In this dynamic the flipping probability is dependent on the transition rate $W(\sigma_i \rightarrow \sigma'_i)$, which is given by the Metropolis prescription as follows

$$W(\sigma_i \rightarrow \sigma'_i) = \begin{cases} e^{(-\Delta E/k_B T)} & \text{if } \Delta E > 0 \\ 1 & \text{if } \Delta E \leq 0 \end{cases}, \quad (3)$$

where ΔE is the change in energy after flipping the spin, $\sigma_i \rightarrow \sigma'_i$, k_B is the Boltzmann constant, and T the temperature of the system. The new state is accepted if $\Delta E \leq 0$, in the case of $\Delta E > 0$ we choose another random number $1 < \xi < 0$ and if $\xi \leq \exp(-\Delta E/k_B T)$ the new state is also accepted, but if none of the conditions are satisfied, we do not change the state of the system. Repeating the Markov process N times, we have one Monte Carlo Step (MCS). In our simulation, we have waited for 2×10^4 MCS for the system to reach the stationary state for all the lattice sizes. We used more 5×10^3 MCS to calculate the thermal averages of the quantities of interest. The average over the samples was done using 25 independent samples for any lattices.

The measured thermodynamic quantities in our simulations are: magnetization per spin m_L , magnetic susceptibility χ_L and reduced fourth-order Binder cumulant U_L :

$$m_L = \frac{1}{N} \left[\left\langle \sum_{i=1}^N \sigma_i \right\rangle \right], \quad (4)$$

$$\chi_L = \frac{N}{k_B T} \left[\langle m_L^2 \rangle - \langle m_L \rangle^2 \right], \quad (5)$$

$$U_L = 1 - \frac{[\langle m_L^4 \rangle]}{3 [\langle m_L^2 \rangle^2]}, \quad (6)$$

where [...] denotes the average over the 25 samples and (...) is the thermal average over the 5×10^3 MCS. The lattice sizes from $L = 24$ to $L = 256$ are simulated and the data are analyzed via the FSS theory. The above-defined quantities obey the following FSS relations in the neighborhood of the critical temperature T_c :

$$m_L = L^{-\beta/\nu} m_0(L^{1/\nu} \varepsilon), \quad (7)$$

$$\chi_L = L^{\gamma/\nu} \chi_0(L^{1/\nu} \varepsilon), \quad (8)$$

$$U_L = U_0(L^{1/\nu} \varepsilon), \quad (9)$$

where $\varepsilon = (T - T_c)/T_c$, and $m_0(L^{1/\nu} \varepsilon)$, $\chi_0(L^{1/\nu} \varepsilon)$ and $U_0(L^{1/\nu} \varepsilon)$ are scaling functions, and β , γ and ν are the magnetization, magnetic susceptibility and length correlation critical exponents, respectively. The derivative of Eq. (9) with respect to the parameter T give us the following scaling relation:

$$U'_L = L^{1/\nu} \frac{U'_0(L^{1/\nu} \varepsilon)}{T_c}. \quad (10)$$

We have determined the critical exponents β/ν , γ/ν and ν from slope of a log-log plot of $m_L(T_c)$, $\chi_L(T_c)$ or $U'_L(T_c)$ versus lattice size L , respectively. We also have used another alternative method to estimate the values of the critical exponents, the data collapse from the scaling functions [20–22].

IV. RESULTS

In this section, we present the results for the magnetic properties of the Ising model on a 2D A-SWN. The Ising model is very useful to identify the phase transitions in magnetic systems. This can be made by observing the behavior of the magnetic susceptibility due to its discontinuously at the critical point and thermodynamic limit. On the other hand, computationally this limit is impracticable, so we use some techniques to study the critical behavior for finite-size lattices [20–22]. One of these techniques is to calculate the temperature $T(\chi_L^{max})$ for the locations of the maxima magnetic susceptibility peaks for each L and to plot versus L^{-1} . The critical temperature can be estimated from an infinite-size extrapolation in according to $T(\chi_L^{max}) - T_c(\infty) = \alpha L^{-1}$. In addition, to here we also have used the crossing of the reduced fourth-order Binder cumulant U_L for different lattice sizes L to identify the critical temperature and the second-order phase transition in the system [23]. For $L \rightarrow \infty$, we have that $U_\infty \rightarrow 2/3$ in the ordered phase, and $U_\infty \rightarrow 0$ in the disordered phase. We observed a singular point independent of the lattice sizes and correspond to the critical point of the phase transitions [20–23]. The critical temperature obtained by this method is in agreement with those obtained from the maxima of the magnetic susceptibility.

In the A-SWN regime ($0 < p \leq 1$), we have used $p = 0.25$, $p = 0.50$, $p = 0.75$ and $p = 1$ to study the critical behavior of the system. The best results are obtained from $p = 1$ and $p = 0.75$, where the majority quantity of the sites contains the same coordination number $z = 5$. In Fig. 2, we can see the finite-size behavior of some thermodynamic quantities, such as the magnetization m_L , the fourth-order Binder cumulant U_L , and the magnetic susceptibility χ_L as a function of temperature T and for several lattice sizes L , in the A-SWN regime with $p = 0.75$. The finite-size behavior is observed when the magnetization vanishes with increasing the temperature T (see Fig. 2(a)) and the magnetic susceptibility presents

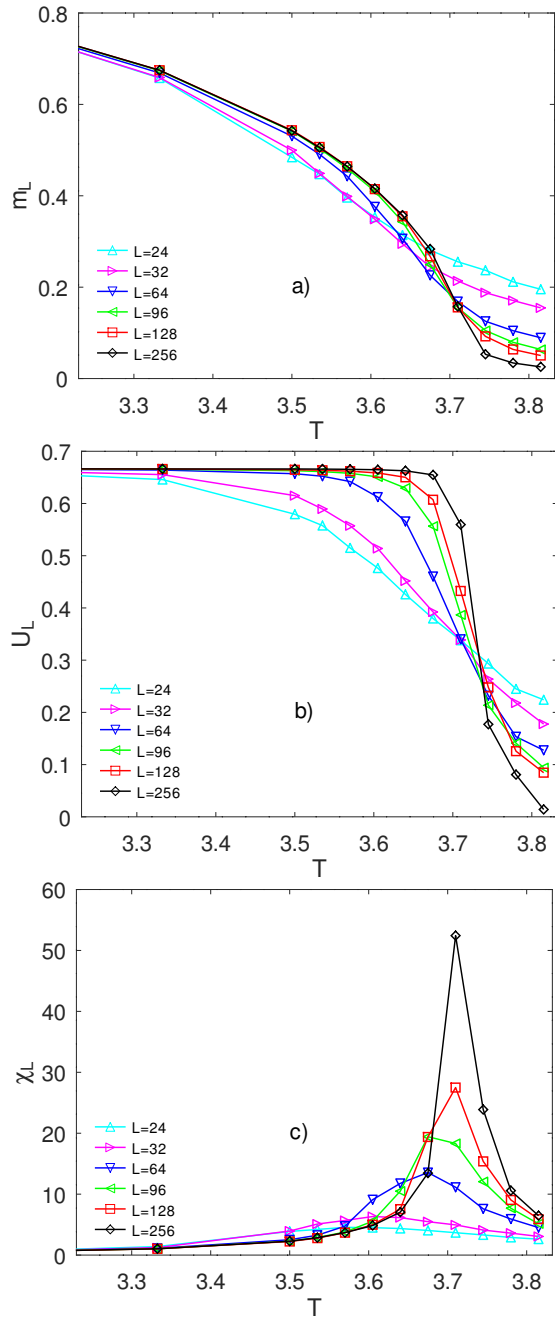


Figure 2. Finite-size behavior of the a) magnetization m_L , b) fourth-order Binder cumulant U_L , and c) magnetic susceptibility χ_L as a function of temperature T for several lattice sizes L , as indicated in the figures. Here, we have used a fixed additive probability $p = 0.75$. The error bars are within the symbol size.

a peak around the critical temperature T_c , which grows in height with the increase of L indicating the existence of a phase transition (see Fig. 2(c)). The position of the magnetic susceptibility peaks can be defined at a pseudo-critical temperature $T(\chi_L^{max})$. The $T(\chi_L^{max})$ approaches $T_c(\infty)$ of the system when $L \rightarrow \infty$. To study the phase transition in more detail, we also used the fourth-order cumulants U_L intersection method to determine the value

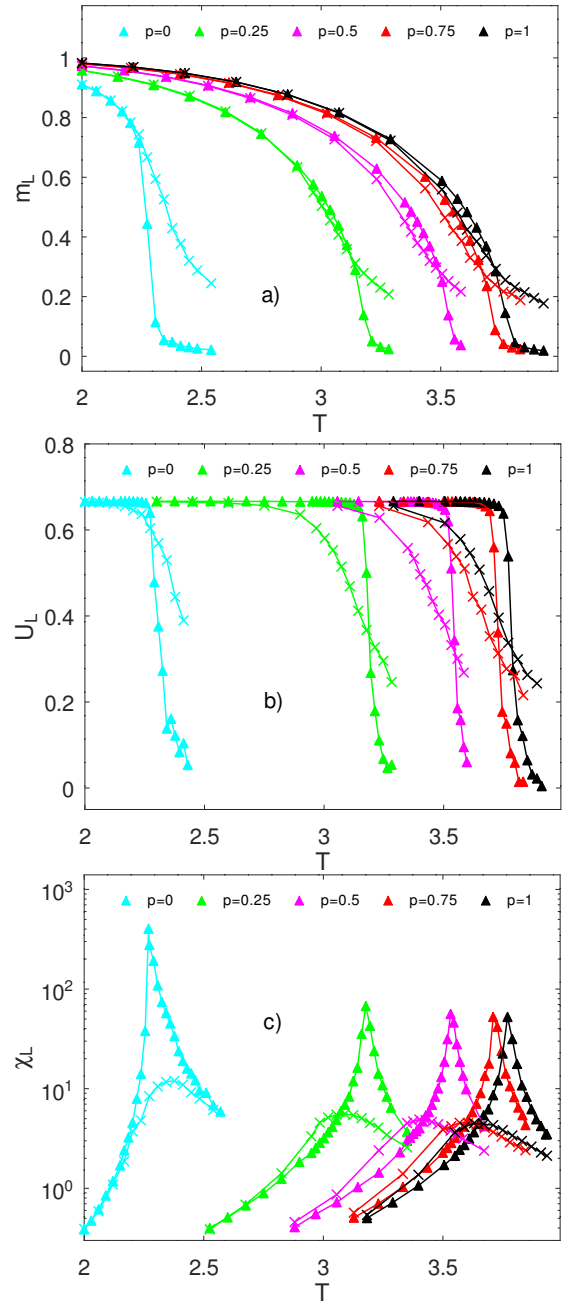


Figure 3. a) Magnetization m_L , b) fourth-order Binder cumulant U_L , and c) magnetic susceptibility χ_L as a function of temperature T for two different lattice sizes $L = 256$ (Δ) and $L = 24$ (\times), and for several values of p , as indicated in the figures. The error bars are within the symbol size.

of temperature at which the transition occurs. In order to find the critical temperature, we display in Fig. 2(b) the cumulants $U_L(T)$ vs temperature T for several system sizes L . For example, our estimate for the dimensionless critical temperature is $T_c = 3.73 \pm 0.02$.

In Fig. 3, we observed the same behavior of the finite-size lattice of the magnetization m_L (Fig. 3(a)), the fourth-order Binder cumulant U_L (Fig. 3(b)), and the

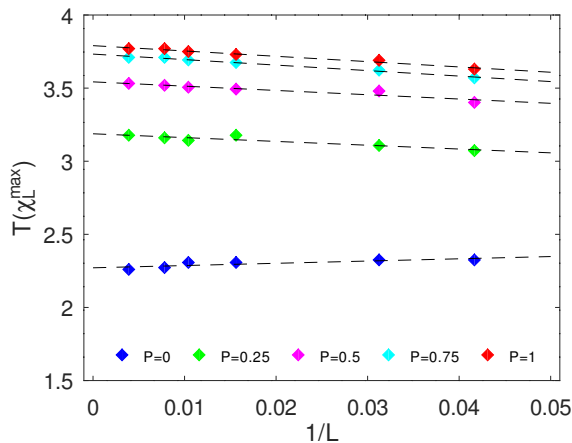


Figure 4. Extrapolation of temperatures obtained by a lattice with the linear size $24 \leq L \leq 256$ as $L \rightarrow \infty$, for different values of p , as indicated in the figures. We have found critical temperature $T_c(\infty)$ for $L \rightarrow \infty$ (see in Table I). The error bars are within the symbol size.

magnetic susceptibility χ_L (Fig. 3(c)) as a function of temperature T for other values of p ($0 \leq p \leq 1$). In this case, we present only two different lattice sizes $L = 256$ and $L = 24$. Together with the values of p in the A-SWN regime ($0 < p \leq 1$), we also calculate $p = 0$, which is a very known result of the two-dimensional Ising model in the regular lattice, and it is calculated here by comparison with the different critical behaviors.

The infinite-size extrapolation of the magnetic susceptibility peaks at the critical point can be seen in Fig. 4 for some values p selected here. The values of $T_c(\infty)$ obtained by extrapolation of $T(\chi_L^{max})$ for the linear size $24 \leq L \leq 256$ with $L \rightarrow \infty$ can be found in Table I, and the T_c^U calculated by the crossing of the U_L curves can be seen in Table II, both for the different values of p . In relation to T_c , we can see an agreement with the two methods utilized here. When we increase the additive probability p , also increase the T_c of the system due to addition of long-range interaction J_{ik} to the system and this consequently increase the mean coordination number of the A-SWN. With $p = 1$ all the sites have one long-range interaction J_{ik} , therefore, the coordination number z is the same obtained in the SW-model studied in reference [19]. We can see that the critical temperature obtained here $T_c(\infty) = 3.79 \pm 0.02$ agrees with that obtained in the Ref. [19], showing that the sublattices do not change the critical behavior of the system and it is subjected to the same random long-range interaction J_{ik} .

We also have constructed the phases diagram showing the behavior of temperature T as a function of the addition probability p , and can be seen in Fig. 5. The phase diagram presents the F ferromagnetic and P paramagnetic phases and the full black line represents a second-order transition line. We can see the critical temperature increases with the addition of J_{ik} , beginning from the standard Ising model in $p = 0$, and increasing log-

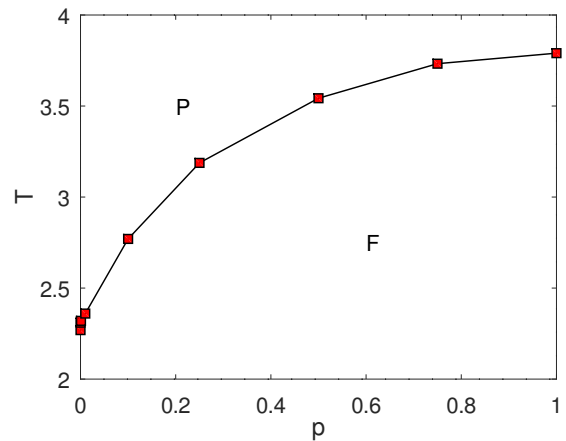


Figure 5. Phases diagram of the Ising model on a 2D A-SWN, in the temperature T vs additive probability p plane. F and P are the ferromagnetic and paramagnetic phases, respectively. The red-square dots represent second-order phase transition points and full black line is a guide to the eyes. The error bars are within the symbol size.

arithmically in order to $T \sim \ln(p^{0.45})$ for $p \gtrsim 0.1$ until $p = 1$.

The critical point and the critical exponents for a phase transition can be determined using the FSS analysis. We calculated the critical exponents of the system by the slope of the best fit in the log-log plot using the scaling relations Eq. (7), (8), and (10). From the slope of the log-log plot for the magnetization m_L at the critical point for the different lattice sizes L as indicated in Eq. (7), we found the ratio $-\beta/\nu$, and can be seen in Fig. 6(a). In the same way, the slope of the log-log plot of the Eq. (8) give us the relation γ/ν (see Fig. 6(b)), and for the ν exponent related to the correlation length of the system, we used the derivative of the cumulant of the scaling relations Eq. (10), where its slope in the log-log plot give us the relation $1/\nu$, see Fig. 6(c) [20–22]. The log-log plot for scaling relations for the some select values of p can be seen in the Fig. 6, which are in the A-SWN regime and for $p = 0$ in contrast to the critical behavior in a regular lattice and the A-SWN. As our interest is in the slope of the log-log plot, we changed the linear coefficients of the straight lines to separate the lines and thus making it easier for the reader to see the fits.

We also have employed another procedure such that a family of curves $m_L(T)$ and $\chi_L(T)$ collapse onto a single curve, the scaling functions $m_0(L^{1/\nu}\varepsilon)$ and $\chi_0(L^{1/\nu}\varepsilon)$ respectively, as well as possible [20–22]. In this procedure, the best fitting can be obtained by adjusting the critical exponents in the log-log plot of the isolated scaling functions as a function of its variable $L^{1/\nu}\varepsilon$. Thus the critical exponents that best collapse the curves are the possible critical exponents of the system, having the verification of the exponent ν_m and ν_χ (ver isso) by the magnetization and magnetic susceptibility collapsed curves, respectively. For the values of T , we have $\varepsilon > 0$ and $\varepsilon < 0$,

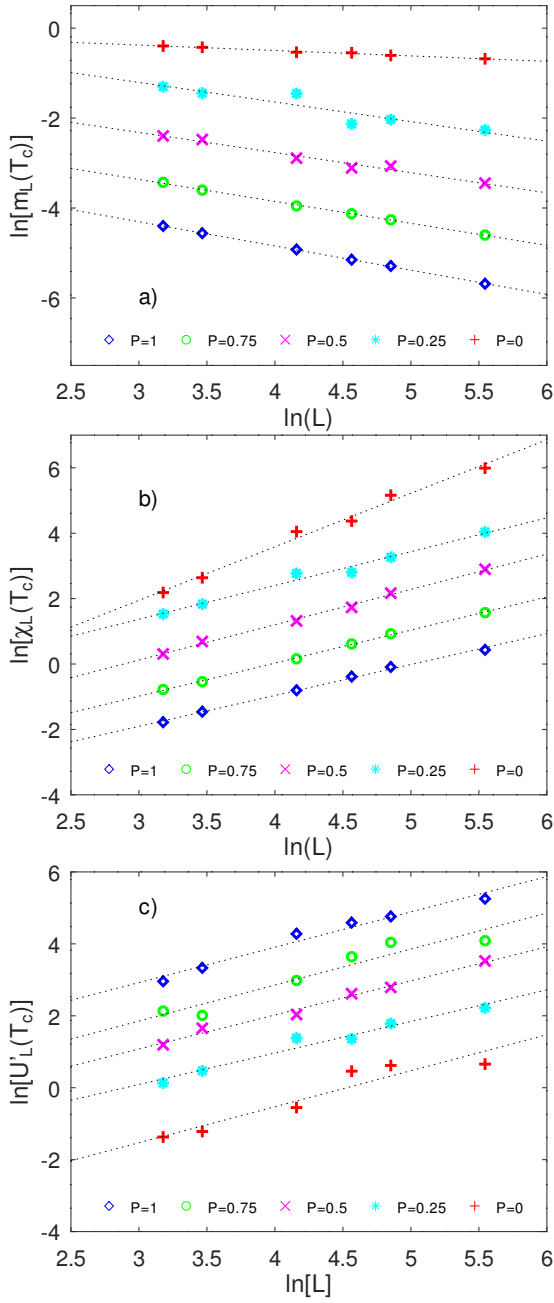


Figure 6. The log-log plots of a) $m_L(T_c)$, b) $\chi_L(T_c)$, and c) $U'_L(T_c)$ vs L , at the critical point and for different values of p , as shown in the figures. The dotted lines are the best fit for the data points. From these slopes, we have obtained the critical exponents β/ν , γ/ν , and ν as can see in Table I. The error bars are within the symbol size.

resulting in two curves on the data collapse, where the best collapse should be near critical point and for the largest values of L , because is in this region that the scale relations are defined.

The best data collapse was obtained for $p = 0.75$, and they are present in Fig. 7. In this figure, we have displayed the collapsed curve for the magnetization $m_L(T)$

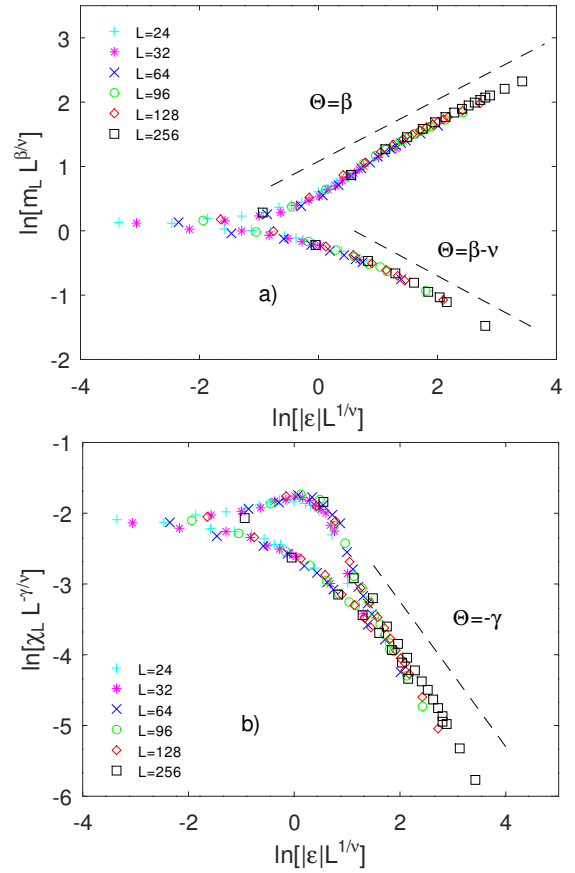


Figure 7. Finite-size scaling (full data collapse) for the a) magnetization m_L and b) magnetic susceptibility χ_L for different values of L as indicated in the figures. The parameter ε is defined by $\varepsilon = (T - T_c)/T_c$. The dashed lines represent the asymptotic behavior of the scaling functions. The optimal values obtained for the critical exponents β , γ , ν_m , and ν_χ can see in Table II for the case $p = 0.75$. The error bars are within the symbol size.

(Fig. 7(a)) and for the magnetic susceptibility $\chi_L(T)$ (Fig. 7(b)), and in both figures we have two curves representing the data with $\varepsilon < 0$ and $\varepsilon > 0$. The data magnetization for $\varepsilon < 0$ corresponds to the slope $\Theta = \beta$, and the data for $\varepsilon > 0$ we have the slope $\Theta = \beta - \nu$. On the other hand, for the magnetic susceptibility in both cases we have the slope $\Theta = -\gamma$, being the superior curve referent to $T < T_c$ and the inferior curve are data for $T > T_c$. For the other values of p , we have obtained the best-fitting and the collapsed curves for the lattice sizes $L = 24$ and $L = 256$, which can be seen in Fig. 8(a) for $m_L(T)$ and in Fig. 8(b) for $\chi_L(T)$.

The results for critical exponents obtained by the best fit of the log-log plots of thermodynamic quantities near T_c are exhibited in Table I and the critical exponents based on the data collapses are shown in Table II. In the both methods we found equivalent values for the critical exponent for each p , being the best results here based on the data collapse, i.e., due to the fact that the values are approximately closer to the values of the Ising model

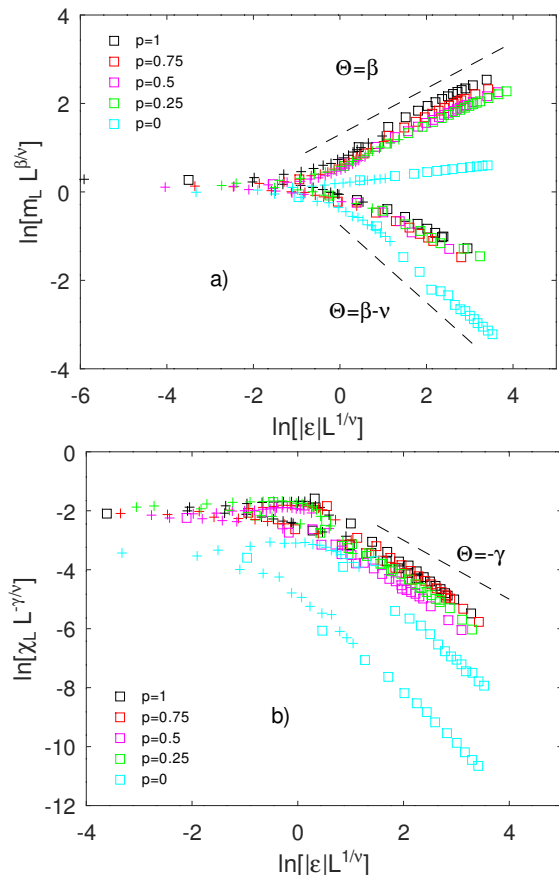


Figure 8. Finite-size scaling (full data collapse) for the a) magnetization m_L and b) magnetic susceptibility χ_L for different values of p as indicated in the figures. The parameter ε is defined by $\varepsilon = (T - T_c)/T_c$. The dashed lines represent the asymptotic behavior of the scaling functions. The critical exponents used here are presented in Table II and they were obtained using the best data collapse for all the lattice sizes. Here, we exhibit only the lattice size $L = 24$ (+) and $L = 256$ (\square). The error bars are within the symbol size.

in the regular lattice. When $p = 0$, we have the known critical exponents of the 2D Ising model (regular square lattice) for exact solutions and Monte Carlo simulations [24] and given by $\beta = 1/8$, $\gamma = 7/4$ and $\nu = 1$. On the other hand, when we increase the addition probability p , the J_{ik} change these critical exponents until to reach the mean-field behavior as observed in Ref. [19], $\beta = 1/2$, $\gamma = 1$ and $\nu = 1/2$ (using $L^2 = N$ in the scaling relations instead of only L). We also can observe a smooth variance of these exponents along the A-SWN regime, tending to the regular lattice Ising model exponents as the p decrease.

We know that the critical exponents are not independent of each other, but related by simple scaling relations. The scaling relation well-called is the hyperscaling relation $d = 2\beta/\nu + \gamma/\nu$ (scaling laws in which the spatial dimension d appears explicitly) and which give us the spatial dimension d of the system [24]. Therefore, with

the hyperscaling relation, we can see that the system has approximately the same critical exponents in the A-SWN regime (see Table I and II for $0 < p \leq 1$) and its spatial dimension is $d \cong 2.0$. The universality class can be defined as the complete set of exponents at the phase transition, as in the case of the second-order phase transition, where very different systems from each other can share the same set of critical exponents. In general, these systems share the same spatial dimensions, symmetries, and range interactions. Thus, here we have a system with the same symmetries (up-down) and spatial dimensionality $d = 2$ but the range of interactions can be different by adding the long-range interactions J_{ik} . Therefore, here we have a system with a set of critical exponents, and consequently indicating a universality class from the mean-field critical exponents of Ising-like systems, for the A-SWN regime ($0 < p \leq 1$).

Table I. Critical exponents obtained by the best fit of the log-log plots of thermodynamic quantities near T_c (see Fig. 6), $T_c(\infty)$ based in the values of the infinite-lattice critical temperature (see Fig. 4) and for the different values of p .

p	β/ν	γ/ν	ν	$T_c(\infty)$
0	0.120 ± 0.007	1.64 ± 0.08	1.00 ± 0.09	2.27 ± 0.03
0.25	0.44 ± 0.08	1.03 ± 0.06	1.14 ± 0.08	3.19 ± 0.04
0.5	0.45 ± 0.03	1.08 ± 0.03	1.05 ± 0.06	3.54 ± 0.04
0.75	0.49 ± 0.01	1.01 ± 0.02	1.00 ± 0.09	3.73 ± 0.01
1	0.54 ± 0.01	0.95 ± 0.02	1.02 ± 0.08	3.79 ± 0.02

V. CONCLUSIONS

In this work, we have developed the Monte Carlo simulations to study of thermodynamic quantities and critical behavior of the Ising model on a 2D A-SWN. With the thermodynamic quantities and the fourth-order Binder cumulant we have obtained the critical point of the second-order phase transitions in the A-SWN regime ($0 < p \leq 1$). The ordered to disordered phase transitions result in a phase diagram from the ferromagnetic F to paramagnetic P phase transitions, in which we can observe an increase in the critical temperature T_c of the system as the addition of the long-range interactions J_{ik} . Through Monte Carlo simulations and finite-size scaling arguments, we calculated the static critical exponents β , γ , and ν , and we concluded that based on the critical exponents, this model is in the same universality class of the pure Ising model in two dimensions on mean-field approximation in the A-SWN regime ($0 < p \leq 1$). However, we also have obtained the critical exponents for the system in the case $p = 0$, and we have observed that the system has a critical behavior from the regular square lattice Ising model with critical exponents calculated using exact calculation and Monte Carlo simulation. Our results, of the change in T_c and the mean-field behav-

Table II. Critical exponents obtained by the best data collapse (see Fig. 7 and Fig. 8), T_c^U based on the crossing of the U_L curves for different lattice sizes L and for the several values of p . The spatial dimension is calculated by hyperscaling relation $d = 2\beta/\nu + \gamma/\nu$.

p	β	γ	ν_m	ν_χ	T_c^U	d
0	0.125 ± 0.002	1.75 ± 0.05	1.00 ± 0.05	1.00 ± 0.05	2.27 ± 0.01	2.0
0.25	0.44 ± 0.04	1.12 ± 0.05	0.95 ± 0.05	1.05 ± 0.09	3.18 ± 0.03	2.0
0.5	0.45 ± 0.03	1.15 ± 0.03	0.95 ± 0.05	1.05 ± 0.03	3.54 ± 0.02	2.05
0.75	0.48 ± 0.02	1.02 ± 0.03	0.98 ± 0.04	0.98 ± 0.04	3.73 ± 0.02	2.02
1	0.52 ± 0.03	1.00 ± 0.04	0.98 ± 0.03	1.00 ± 0.03	3.79 ± 0.01	2.06

ior is in agreement with the observed behavior of disorder with shortcuts added to the Ising model in R-SWN and A-SWN [5, 14, 16, 17, 19]. Therefore, the direction in the long-range interactions between sublattices of the

network, do not change the SWN behavior, being that the Ising Model on a 2D A-SWN scales logarithmically as a function of p to the mean-field critical behavior.

-
- [1] S. Mingram. Psychol. Today, 2, 60 (1967);
- [2] D. J. Watts and S. H. Strogatz. Nature, 393, 440 (1998);
- [3] D. J. Watts, Small Worlds (Princeton University Press, Princeton, NJ, 1999);
- [4] M. E. J. Newman and D. J. Watts. Phys. Rev. E, 60, 7332 (1999);
- [5] A. Barrat and M. Weigt. Eur. Phys. J. B, 13, 547 (2000);
- [6] M. E. J. Newman. SIAM Rev., 45, 167 (2003);
- [7] R. Albert and A.-L. Barabási. Rev. Mod. Phys., 74, 47 (2002);
- [8] C. Moore and M. E. J. Newman. Phys. Rev. E, 61, 5678 (2000);
- [9] A. D. Sánchez, J. M. López, and M. A. Rodríguez. Phys. Rev. Lett., 88, 048701 (2002);
- [10] M. Dupont and N. Laflorencie. Phys. Rev. B, 103, 174415 (2021);
- [11] B. J. Zubillaga, A. L. M. Vilela, M. Wang, R. Du, G. Dong, and H. E. Stanley. Sci. Rep., 12, 282 (2021);
- [12] E. M. S. Luz and F. W. S. Lima. Int. J. Mod. Phys. C, 18, 1251 (2007);
- [13] A. Pękalski. Phys. Rev. E, 64, 057104 (2001);
- [14] H. Hong, B. J. Kim, and M. Y. Choi. Phys. Rev. E, 66, 018101 (2002);
- [15] F. W. S. Lima. RMES, 03, 000553 (2017) ;
- [16] C. P. Herrero. Phys. Rev. E, 65, 066110 (2002);
- [17] M. Gitterman. J. Phys. A, 33, 8373 (2000);
- [18] J. V. Lopes, Y. G. Pogorelov, J. M. B. L. dos Santos, and R. Toral. Phys.
- [19] X. Zhang and M. Novotny. Braz. J. Phys., 36, 3A (2006); Rev. E, 70, 026112 (2004);
- [20] K. Binder and D. W. Heermann. *Monte Carlo Simulation in Statistical Physics*. An Introduction, 6rd ed. (Springer, Cham, Switzerland, 2019);
- [21] K. Binder and D. P. Landau. *A Guide to Monte Carlo Simulations in Statistical Physics*, 4rd ed. (TJ International Ltd, Padstow, UK, 2015);
- [22] L. Böttcher and H. J. Herrmann. *Computational Statistical Physics*, 1rd ed. (Cambridge University Press, NewYork, EUA, 2021);
- [23] S.-H. Tsai and S. R. Salinas. Braz. J. Phys., 28, 1, (1998);
- [24] G. Ódor. Rev. Mod. Phys., 76, 663 (2004).

ACKNOWLEDGMENTS

This work was partially supported by the Brazilian agencies CNPq, UFMT and FAPEMAT.